Realizing an ultra-wideband backward-wave metamaterial waveguide

S. S. Seetharaman, B. Tremain, W. L. Barnes, and I. R. Hooper*
Department of Physics and Astronomy, University of Exeter, Stocker Road, Exeter, EX4 4QL United Kingdom

(Received 20 June 2018; revised manuscript received 14 November 2018; published 5 December 2018)

Electroinductive waves have emerged as an attractive solution for designing metamaterials that support backward propagating waves. Stacked metasurfaces etched with complementary split-ring resonators (CSRRs) have also been shown to exhibit a broadband negative dispersion. We demonstrate, through experiment and numerical modeling, that the operational bandwidth of a CSRR metamaterial waveguide can be improved by restricting cross-polarization effects in the constituent meta-atoms. We report a fractional bandwidth of >56%, which, to the best of our knowledge, is broader than any previously reported value for an electroinductive metamaterial. We present a traditional coupled-dipole toy model as a tool to understand the field interactions in CSRR-based metamaterials, and to explain the origin of their negative dispersion response.

DOI: 10.1103/PhysRevB.98.235408

I. INTRODUCTION

Metamaterials are a special class of artificial materials composed of meta-atoms, whose size and spacing are significantly smaller than the wavelength of the light with which they interact. Electromagnetic metamaterials may have their effective values of the permittivity and permeability simultaneously negative, something not found in nature. Such double-negative metamaterials have a negative refractive index. As pointed out by Veselago [1], a negative refractive index leads to unique effects such as the inversion of Snell's law, backward propagation of waves, and reverse Cerenkov radiation. The first conceptual realization of a negative index metamaterial (NIM) was achieved by combining two single negative materials: a wire array exhibiting negative permittivity and an array of split-ring resonators (SRRs) [2] exhibiting negative permeability [3], in an overlapping frequency region. Shelby *et al.* experimentally demonstrated that this combination indeed exhibited a negative refractive index [4].

The dispersion characteristics of the NIMs obtained using negative material parameters [5] and using an equivalent circuit approach [6] both revealed the existence of a negative dispersion passband that supports backward propagating waves as predicted by Veselago in [1]. The authors of [6] investigated the dispersion characteristics of the NIM's equivalent circuit model to analyze the system's resonant response when the electromagnetic wave propagating in free space and the SRR array (where the neighboring SRRs are coupled to one another) were uncoupled. This analysis revealed that the SRR medium on its own could act as a backward-wave medium (without negative refractive index) by virtue of the magnetoinductive (MI) coupling between the SRRs, which was already a familiar concept by then [7,8]. The MI waves have since paved the way for the emergence of several interesting applications such as magnetoinductive waveguides [8], magnetoinductive lenses for subwavelength focusing of electromagnetic radiation [9,10], and in general as wireless data transfer devices.

A parallel idea to the guiding of electromagnetic waves via magnetoinductive coupling is instead to use an electroinductive (EI) waveguide composed of electrically coupled complementary split-ring resonator (CSRR) meta-atoms [11], something that can also be implemented in general for wireless power transfer applications [12]. These EI metamaterials also exhibit a negative dispersion and backward-wave propagation. Some of the other novel applications that have emerged from the electroinductive waveguide (EIW) concept are oriented towards designing broadband backward-wave metamaterials using stacked CSRR metasurfaces [13] and active metamaterial particle accelerators [14].

The MI devices exhibit positive or negative dispersion depending on the sign of the mutual inductance between the SRRs, which in turn depends on the relative arrangement between SRRs being axial or planar [8]. On the other hand, the mutual capacitive effects in EIW devices have been shown to always result in a negative dispersion [13]. In the works on magnetoinductive waveguide (MIW) and EIW devices, the general observation is that axially coupled meta-atoms of either kind interact more strongly than in the planar configuration, thereby resulting in broader operational bandwidth in devices constructed from axially stacked meta-atoms [8,13]. While applications such as magnetoinductive metamaterial lenses benefit from narrow-band device operation, waveguides, and wireless data transfer devices would benefit from having a broadband operation. The device fractional bandwidth of the stacked CSRR metamaterial in [13] of about 26% is one of the broadest values reported in the literature that we are aware of. However, we note that the stacked CSRR metamaterial's operational bandwidth is quite sensitive to the lattice period along the direction of stacking and, as acknowledged by the authors, negative dispersion could be achieved only for small stacking distances between the metasurfaces.

The motivation for our work is twofold. The key to manipulating the operational bandwidth in metamaterials comes down to understanding the nature of the fields in

*i.r.hooper@exeter.ac.uk

TABLE I. Top row: the electric and magnetic net dipole moments associated with the fundamental resonance of different ring resonators. Bottom row: the electric and magnetic dipole moments in the top and bottom half spaces of the corresponding complementary resonators. Note: The complementary resonators exhibit zero net dipole moments since the modes consist of equal and opposite *local* dipole moments on either side of the rings, as shown. When considering the interactions between adjacent complementary resonators, it is these local dipole moments in the spaces between the resonators that need to be considered.

Single-ring (bianisotropic)	Single-ring (nonbianisotropic)	Double-ring (bianisotropic)	Double-ring (nonbianisotropic)
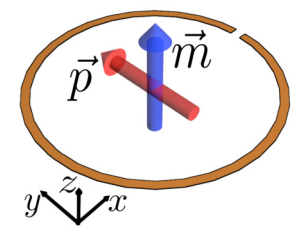	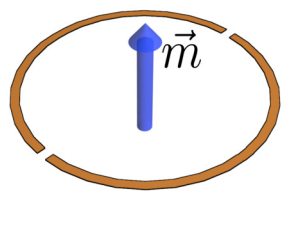	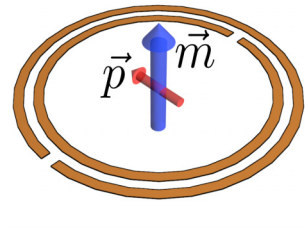	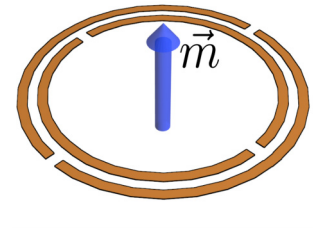
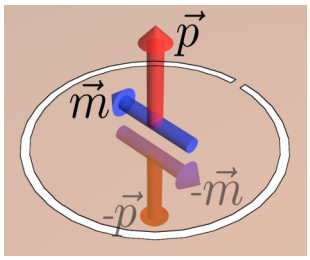	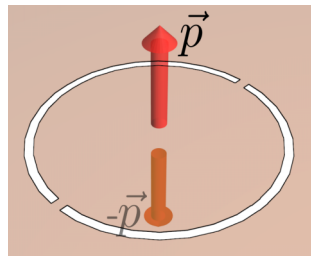	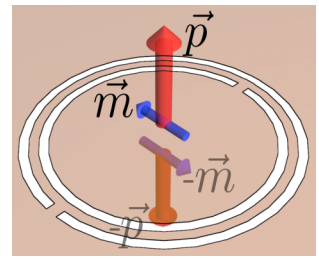	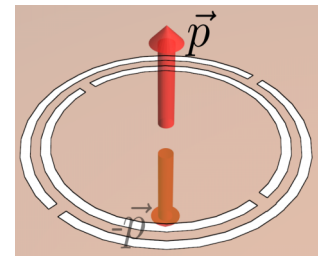

individual meta-atoms as much as understanding the field interactions between them. It is well known from the literature that the conventional SRR (originally proposed in [2]) and by Babinet's principle, the CSRRs (proposed in [11]) are bianisotropic. We have observed previously that the coupling strength between bianisotropic SRRs is reduced due to the competition between the field interactions [15]. The first motivation therefore is to analyze the field distribution of an individual CSRR meta-atom and suggest a nonbianisotropic design that would in turn enhance interelement interactions and the metamaterial's operational bandwidth. The second motivation is to help complete the understanding of the field interactions in the complementary metamaterial structures. The standard approach to visualizing the interactions in complementary metamaterials adopted in the literature has mostly been via a circuit analysis. Here, we use a coupled-dipole picture to describe the field interactions between complementary meta-atoms; we hope this approach will complement and extend the understanding gained using the standard circuit approach.

Below, in Sec. II, we discuss the nature of the resonant response of various SRRs and CSRRs, elaborating on the method to eliminate bianisotropy by making appropriate design choices. We then analyze and compare one-dimensional (1D) axially stacked complementary metamaterials constructed using CSRR meta-atoms, our purpose being to highlight the improvement in operational device bandwidth; this is done in Sec. III. In Sec. IV, we employ a simple toy model of the dipole interaction to explain the origin of negative dispersion in CSRR-based metamaterials (both bianisotropic and nonbianisotropic) and our observations. In the final section, we compare the change in operational bandwidths of a 1D metamaterial stack made of conventional CSRRs with that of nonbianisotropic CSRRs, as a function of longitudinal stacking periodicity.

II. DESIGN APPROACH TO ELIMINATE BIANISOTROPY

A complementary split-ring resonator (CSRR) is realized by replacing the metallic portions of a SRR with air gaps and the air surrounding the SRR in its plane by metal, so as to create a negative image of the SRR [11]. The top row of Table I shows some of the popular configurations of split-ring resonators: the single-ring SRR, the nonbianisotropic version of the single-ring SRR, the standard double-ring SRR [2], and its nonbianisotropic version, the so-called double-split SRR (DSRR) [16], along with the net dipole moments associated with the fundamental resonance of each resonator, shown as red (electric) and blue (magnetic) arrows. The bottom row in Table I shows the complementary resonators, each being a negative image of the standard resonators in the top row. The electric and magnetic dipole moments on the top and bottom half spaces of the complementary resonators (above and below the plane of the meta-atom) arise because of the presence of the central metallic disk in the complementary structures, and are shown by the red and blue arrows, respectively. The opposite polarities of the field dipoles on either side of the CSRRs result in a zero net dipole moment for each CSRR. The coordinate system displayed in the first meta-atom window of the table is common to all the tabulated meta-atoms, the z axis coinciding with the out-of-plane axis of the meta-atoms.

The single-ring SRR in the top row of Table I is the simplest bianisotropic SRR configuration with a net electric dipole moment in the plane of the SRR, and a net magnetic dipole moment out of its plane. The double-ring SRR is a planar combination of two nonidentical single-ring SRRs, with their splits placed symmetrically opposite to each other. This geometry serves to achieve a high-Q-factor resonance through an almost perfect cancellation between the electric fields at the splits, thereby making the meta-atom's response at resonance predominantly magnetic. The double-ring structures are also attractive as their fundamental resonance occurs at a much lower resonance frequency than those of the constituent single rings, they are thus more subwavelength in character. The duality of fields between the SRR and CSRR meta-atoms due to Babinet's principle has been established and treated in depth in the literature [11,16–18] and is also seen from Table I. The corresponding CSRRs for the single-ring and double-ring geometries, as seen in the bottom row of Table I, exhibit out-of-plane electric dipole moments and in-plane magnetic dipole moments, as dictated by Babinet's principle. The local dipole moments on either side (top and bottom) of a complementary resonator are equal in strength and oppositely polarized as represented in Table I, resulting in a zero net dipole moment. Despite the zero net dipole moment, the CSRRs can be excited by time-varying local fields on one (either) side and can interact with other adjacent CSRR meta-atoms through their excited near fields. Therefore, when analyzing the interactions between adjacent complementary resonators, the local dipole moments of the resonators in the space between them need to be considered.

The bianisotropic nature of the CSRR meta-atom results in cross-polarization effects which are not advantageous for designing metamaterials with enhanced meta-atom interactions [19]. In particular, in our previous work [15], a detailed analysis of the coupling between bianisotropic SRRs revealed that the interaction strength is affected strongly by competition between electric and magnetic field interactions. In a metamaterial, a reduced interaction strength among the multiple constituent meta-atoms would reduce the operational bandwidth and would also make the dispersion sensitive to changes in the lattice period. Our main motivation is therefore to exclude bianisotropy from our design so as to strengthen the interelement interactions.

The necessary condition for the existence of bianisotropy in a metamaterial is the absence of inversion symmetry in the geometry of the constituent meta-atoms [16,20–23]. To demonstrate this condition, consider for example the single-ring bianisotropic structure from Table I. Choosing the yz plane as its center of inversion and transforming $x \rightarrow -x$ results in a meta-atom that does not coincide with the meta-atom before inversion. If the original and the inverted meta-atoms were to be excited using the electric field component (E_y) of a normally incident electromagnetic wave, the electric dipoles excited at their splits would both be polarized along the same direction at any given instant. However, the electric currents resulting from the flow of charges between the ends of the splits are directed opposite to each other in the original and in the inverted meta-atoms, resulting in oppositely polarized magnetic dipoles. The same conclusion can be arrived at by imagining the meta-atom being excited by just the magnetic field component (H_z) of an electromagnetic wave traveling in the y direction or being simultaneously excited by the electric and magnetic field components (E_y and H_z) of an electromagnetic wave traveling in the x direction. The lack of inversion symmetry can similarly be identified in the double-ring bianisotropic structure of Table I. Naturally, the corresponding complementary meta-atoms of these SRRs possess the same lack of inversion symmetry and are therefore also bianisotropic.

The key to removing bianisotropy is to impose an inversion symmetry. In the single-ring nonbianisotropic SRR of the top row, the inversion symmetry is enforced by having two symmetrically placed splits. Thus, the fundamental resonant mode of this meta-atom has an out-of-plane net magnetic dipole moment but the electric contributions from the splits perfectly cancel each other out, as seen from Table I. The same principle can be extended to the double-ring geometry by introducing symmetric splits in both the inner and outer split rings. The inner ring is rotated by 90° so that the inversion symmetry is preserved while avoiding interference between the inner and the outer rings' electric fields. Their complementary nonbianisotropic counterparts from the bottom row of Table I are seen to have only local electric dipole moments on either side.

In Sec. IV, we shall show, using a toy dipole model, how the electric field interactions between regular (bianisotropic) or nonbianisotropic double-ring CSRR meta-atoms in a metamaterial result in negative dispersion. We shall also show that the magnetic fields of the bianisotropic double-ring CSRR meta-atoms, though weaker than in the single-ring CSRRs, interact strongly enough to reduce the bandwidth of the negative dispersion passband.

III. DESIGN AND CHARACTERIZATION OF THE 1D METAMATERIAL

The design process for the nonbianisotropic CSRR meta-atom to be used in our study was performed using a commercial finite element modeling software, COMSOL MULTIPHYSICS, making use of its eigenmode solver. A color photograph of one of the fabricated nonbianisotropic CSRR meta-atoms is shown in Fig. 1(a). It can be seen that the continuous metal sheet surrounding the split-ring-shaped slots is truncated to a circular disk, for easier experimental near-field detection of the supported modes. Due to this deviation from the ideal, the electric response of the meta-atom is slightly different to that of the untruncated complementary meta-atom because part of the electric field fringes to the edges. The collective electric response of this modified nonbianisotropic CSRR (MNB-CSRR) meta-atom can, however, still be represented via local electric dipole moments as shown in Table I.

The dimensions of the design parameters for the meta-atom can be found in Fig. 1(a). The meta-atoms were supported by the commercial Astra MT77 substrate which was 1.5 mm thick. The relative permittivity of this material, as taken from the manufacturer's data sheet, is $3(1 + 0.0017i)$ and constant in the range 1–20 GHz. This meta-atom design has a resonance frequency of 1.92 GHz, as calculated using COMSOL. However, in our 1D axially stacked metamaterial, the resonators are effectively embedded in substrate material. To see

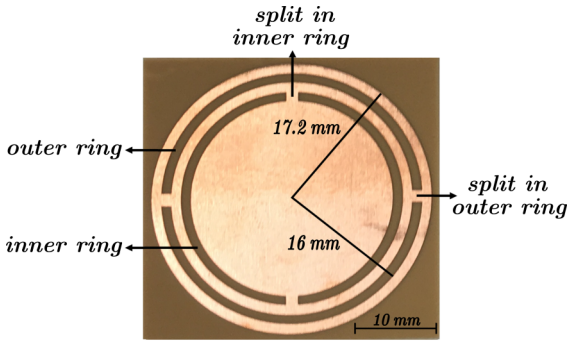

(a)

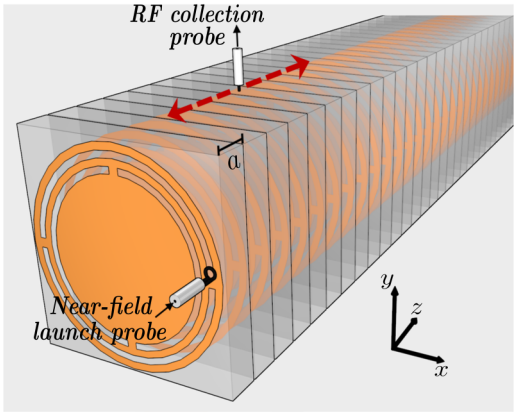

(b)

FIG. 1. (a) A color photograph of the MNB-CSRR meta-atom as fabricated. The splits in both the slots measure 1.5 mm of height and the slots are 1.2 mm wide. The circular metal disk has a radius of 17.2 mm and the outer split-ring-shaped slots have an external radius of 16 mm. The metallic regions between the inner and outer slots is 1.2 mm wide. (b) Schematic of the experimental setup used to excite and detect the fundamental mode of the one-dimensional metamaterial, with period $a = 1.5$ mm. The substrate material has been rendered translucent to reveal the periodic structure. A near-field loop antenna excites the magnetic near field of the 1D metamaterial stack, and a stripped coaxial probe traverses the length of the stack to scan and record the electric near field above it, along the z direction (shown dashed red). Both the launch antenna and the probe are connected to a vector network analyzer.

the effect of this environment on the resonance frequency of a single resonator, we ran a modified COMSOL eigenmode model with two Astra MT77 blocks 20 mm thick each, sandwiching a single MNB-CSRR meta-atom. The meta-atom's resonance frequency in this altered environment was found to be reduced to 1.43 GHz.

A two-dimensional (2D) array of MNB-CSRRs was fabricated commercially by a local PCB manufacturer Graphic PLC, on a commercial Astra MT77 substrate 1.5 mm thick, clad with 35 μm of copper. A layer of photoresist was coated on top of the copper layer and the design of our MNB-CSRR transferred into the resist by laser direct imaging. The photoresist was subsequently developed and the regions of metal thus exposed were etched away using ferric chloride. The individual MNB-CSRRs were then cut from the panel, and the 1D metamaterial was constructed by axially stacking 90 MNB-CSRRs with a periodicity of 1.5 mm, as shown in Fig. 1(b).

The modes supported by the 1D metamaterial stack were excited via their near fields using a loop antenna positioned for optimum coupling as shown in Fig. 1(b). A second antenna, in this case a simple section of stripped coaxial cable, was used to probe the electric near field above the metamaterial stack, as a function of distance along the stack direction shown by the dashed red arrows. Both the launch antenna and the collection probe were connected to the ports of a vector network analyzer (VNA). Despite the suppression of an effective magnetic dipole in the structure, optimally positioning the loop antenna in the vicinity of its magnetic near-field facilitates good coupling into the mode. The coaxial probe recorded the local electric field strength in the frequency range of 1 to 1.9 GHz.

A sample spatial electric field map plot in the inset of Fig. 2(a) shows the real part of the recorded complex electric field distribution at a frequency of 1.43 GHz. The main plot of Fig. 2(a) shows the Fourier transform determined from the complex-valued instantaneous spatial electric field at 1.43 GHz, plotted as a function of wave vector along the z direction. Combining the Fourier transforms of the spatial electric field maps over the range of measured frequencies results in the dispersion diagram shown in Fig. 2(b). The resonant mode that is observed in the diagram has a negative gradient of dispersion (negative group velocity) for positive values of wave vector (positive phase velocity), indicating that the mode is negatively dispersive.

To validate the experimental data, the MNB-CSRR metamaterial stack was modeled in COMSOL MULTIPHYSICS. The eigenvalue solver was used to identify the complex eigenfrequencies of the system as a function of wave vector along the stacking (z) direction, with losses included in both the dielectric substrates and the metal of the resonators. The real parts of the eigenfrequencies are overlain on the experimental data in Fig. 2(b) as red triangular markers.

In order to compare the negatively dispersing modes of nonbianisotropic and bianisotropic systems, we compared our MNB-CSRR stack with an equivalent CSRR stack. A model of a CSRR stack was built in COMSOL with a period and boundary conditions identical to that of our MNB-CSRR system. The design parameters, namely, the width of the slots, the height of the splits, and the radius of the slots and the circular disk, were exactly half of those used in our MNB-CSRR design. This was to ensure that the passband of the negatively dispersing mode of the CSRR stack was centered at 1.43 GHz, the same as for the MNB-CSRR stack. The real parts of the eigenfrequencies for the CSRR stack are overlaid on the experimental data in Fig. 2(b) as blue triangular markers. We see that the mode supported by the MNB-CSRR stack has a greater bandwidth than that supported by the CSRR stack. The fractional bandwidths for each were calculated using

$$\mathrm{FBW} = \frac{\Delta f}{f_c}, \tag{1}$$

where FBW is the fractional bandwidth, Δf is the observed bandwidth, and f_c is the central frequency of the band. Using the data from Fig. 2(b), the FBW for the mode supported

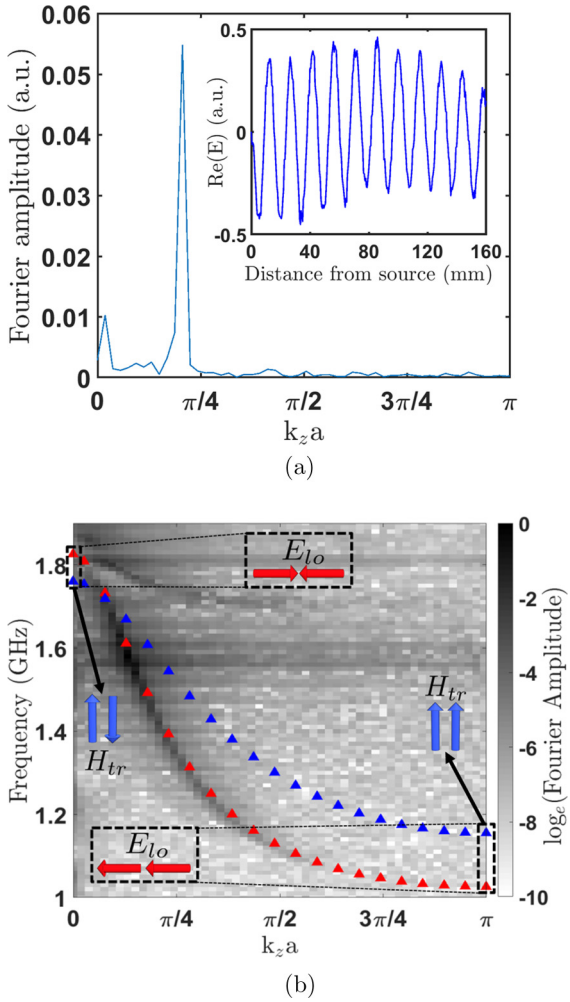

FIG. 2. (a) Fourier transform of the complex spatial electric field distribution at 1.43 GHz, revealing the amplitude of the frequency component as a function of wave vector along the stacking direction. (Inset) Real part of the complex instantaneous electric field at 1.43 GHz plotted as a function of distance from the source along the 1D stack. The excitation source was at 0 mm on the plot. The electric field was recorded in steps of 0.75 mm. (b) Fourier amplitude of the complex spatial electric field map, plotted as a function of frequency and wave vector along the stacking direction. The red and blue triangles indicate the real parts of the eigenfrequencies obtained from COMSOL MULTIPHYSICS models of the MNB-CSRR and CSRR stacks, respectively. The electric field interactions corresponding to $k_z = 0$ and π/a (Brillouin zone boundary) for the negatively dispersing modes are highlighted by the dotted black boxes.

by the CSRR structure is 41.5%, while that of the MNB-CSRR stack is 56.3%. To the best of our knowledge, this is broader than any reported value for magnetoinductive or electroinductive metamaterials.

We also calculated the group velocities [$v_g = \mathrm{Re}(d\omega/dk)$] of the modes from the modeled complex eigenfrequency data as per Fig. 2(b). These are plotted as a function of the longitudinal wave vector k_z in Fig. 3. The wave-vector axis is indicated by $-k_z a$ representing the negative wave-vector direction. This choice of axis is used to indicate that the group velocity is always positive in a material since the power must

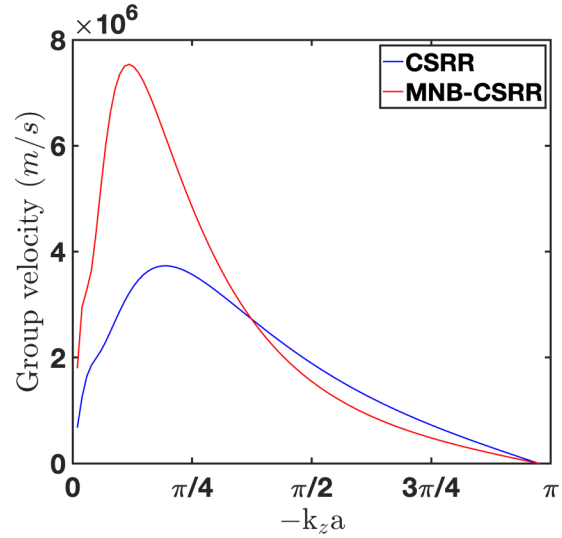

FIG. 3. The group velocities for the negatively dispersing modes of the CSRR and MNB-CSRR waveguides.

always propagate away from the source. The phase velocity in the backward-wave medium is directed opposite to the group velocity and hence the wave vector is negative.

The maximum group velocity of the mode supported by the MNB-CSRR stack is approximately twice that of the mode supported by the CSRR stack. The electroinductive waves are able to travel faster in the MNB-CSRR stack owing to the enhanced coupling in the structure. This can be understood by drawing a comparison to the propagation of elastic waves in solids. The greater the stiffness of a material, i.e., the stronger the atoms of the material are bound to one another, the higher the velocity of the elastic wave.

Finally, we also calculated the attenuation constants of the modes for both the MNB-CSRR and CSRR waveguides. Attenuated modes are commonly described by a real frequency and a complex-valued propagation constant $k_r + ik_i$. To numerically solve this problem with periodic boundary conditions, we incorporate the loss inside a complex frequency $\omega_r + i\omega_i$ while maintaining a real-valued propagation constant k_r with Eq. (2) [24,25]:

$$k_i = \frac{\omega_i}{v_g}, \tag{2}$$

where v_g is the group velocity and ω_i and k_i are the imaginary parts of the complex eigenfrequency and the attenuation constant, respectively. The attenuation constants as a function of frequency are shown in Fig. 4.

The mid-band attenuation constant value of 2.8 m^{-1} for the MNB-CSRR corresponds to a power loss of approximately 12.2 dB/m. Although this may at first seem rather large, it corresponds to a loss per period of only 0.03 dB/m, which compares very favorably with other metamaterial waveguides [26,27]. We also note the following: the vast majority of the losses occur within the dielectric substrates, and could thus be reduced by using thinner substrates and air gaps; and that comparisons to other metamaterial waveguides are rather difficult since studies have tended to focus on waveguides that support modes at much lower frequencies, and in general these

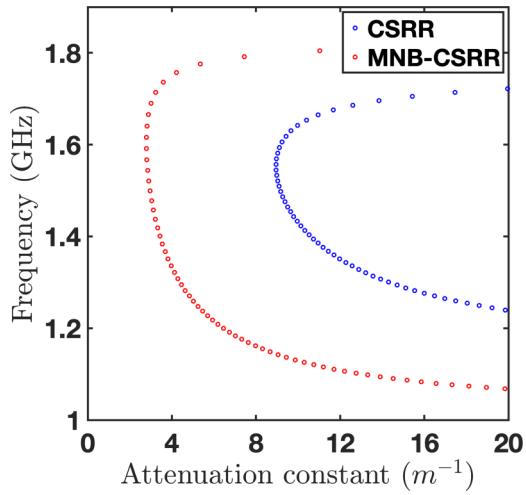

FIG. 4. The attenuation constant for the MNB-CSRR and CSRR waveguides calculated using the modeled dispersion and group velocity data from Figs. 2(b) and 3.

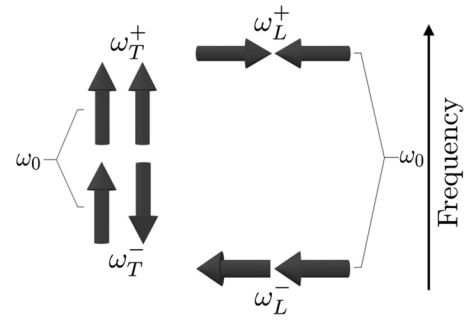

FIG. 5. A schematic showing the splitting of the coupled modes of a pair of dipoles for both transverse (left) and longitudinal (right) orientations of the dipole moments. The magnitude of the frequency splitting is larger when the dipoles are coupled longitudinally.

modes are positively dispersing. In order to provide a fair comparison, we also calculated the attenuation constants for the equivalent CSRR waveguide as described previously. The mid-band attenuation of our MNB-CSRR–based waveguide is approximately 3.2 times smaller than that of the CSRR-based waveguide.

IV. A TOY DIPOLE INTERACTION MODEL TO ANALYZE THE NATURE OF FIELD INTERACTIONS

The observation from the experimental and computational results confirms our expectation that the fractional bandwidth of the negatively dispersive mode in the MNB-CSRR stack exceeds that in the CSRR stack. The interaction among the meta-atoms in the bianisotropic medium is weakened by the competition between the electric and magnetic interactions, as expected. The weakened interaction strength results in the narrowing of the fractional bandwidth, and a smaller group velocity. In this section, we present a toy coupled-dipole model of the field interactions between the complementary meta-atoms as a tool to help explain the origin of negative dispersion in these media, and the impact of bianisotropy on the operational bandwidth of the negative dispersion passband in the CSRR stack. Finally, the effect of near-field interactions is briefly discussed.

First, we discuss the general rules of dipole coupling approach in general. In the simple case of two dipoles, the strength of the coupling between them depends upon their separation and upon their relative orientation; the coupling can be either longitudinal or transverse in nature, as shown in Fig. 5. These coupled modes, whether longitudinal or transverse, correspond to aligned or antialigned dipole moments. For transversely coupled dipoles, the symmetric arrangement (aligned dipole moments) is the higher-energy solution and the antisymmetric arrangement (antialigned dipole moments) is the lower-energy solution; for longitudinally coupled dipoles, this situation is reversed. For a given separation, the frequency difference between the coupled modes is greater for longitudinally coupled dipoles than for transversely coupled dipoles [28].

In the equivalent circuit treatment of CSRR-based metamaterials, the negative dispersion is attributed to the positive mutual capacitance between the resonators [13]. If instead we wish to understand the negative dispersion in terms of field interactions, we need first to consider the relative electric field orientations between two neighboring complementary meta-atoms in the stack, as shown in Figs. 6(a) and 6(b). The view shown in Fig. 6 is from the side of the 1D stack looking along the x direction. As established in Sec. II, this coupled electric dipole picture can be used to understand the electric field interactions in *both* the CSRR and MNB-CSRR stacks. The relative field distributions shown in Figs. 6(a) and 6(b) correspond to the resonant frequencies of the stack associated with wave vectors $k_z = 0$ and π/a (at the Brillouin zone boundary), where a is the longitudinal stacking periodicity. The reason for this choice is that these are the frequencies at the band edges.

At $k_z = 0$, the wavelength of the electroinductive wave in the 1D stack, $\lambda|_{k_z=0} = \infty$, i.e., the fields of the meta-atoms in the stack are all in phase. Whether the resonance frequency associated with this configuration is higher or lower than the resonance frequency of the individual meta-atoms is determined by the relative dipole orientations. As seen in Figs. 6(a) and 6(b), the local electric dipole interactions between the complementary meta-atoms in the 1D stack are represented by longitudinal relative orientations of the dipoles, as highlighted by the dotted blue boxes. By comparing the relative dipole orientation in Fig. 6(a) to those in Fig. 5, we see that the antisymmetric longitudinal orientation favors a higher-energy solution. The antisymmetric longitudinal dipole pair is marked on Fig. 2(b) at $k_z = 0$, highlighted by the dotted black box.

At the Brillouin zone boundary where $k_z = \pi/a$, the fields of each meta-atom are π out of phase with those of its nearest neighbors. Figure 6(b) shows that the relative dipole orientation between the longitudinal electric field components of the adjacent meta-atoms is symmetric in this case, again as highlighted by the dotted blue box. By comparing this to Fig. 5, we see that the longitudinally coupled symmetric orientation corresponds to a lower-energy solution. In Fig. 2(b), this dipole orientation is marked at the frequency position

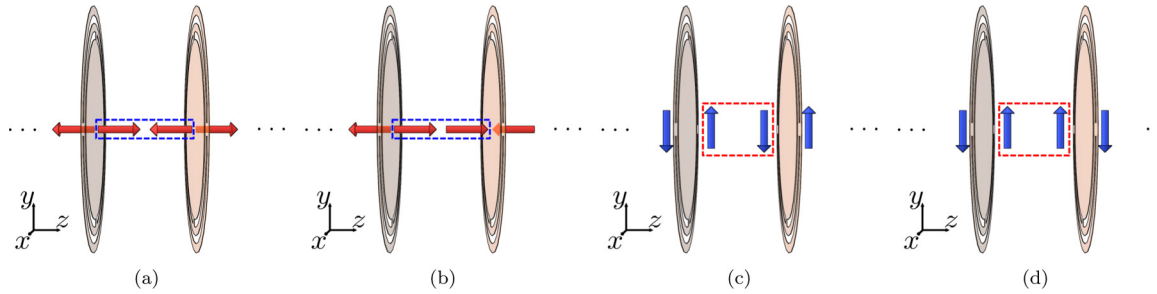

FIG. 6. Relative orientations of the coupled electric dipole moments [(a) and (b)] between two MNB-CSRR (or CSRR) meta-atoms in the 1D stack. The antisymmetric longitudinal dipole arrangement in (a) corresponds to $k_z = 0$ in the periodic medium favoring a higher-energy solution. The symmetric longitudinal dipole arrangement in (b) corresponds to $k_z = \pi/a$ (a period) favoring a lower-energy solution. (c), (d) Show the antisymmetric and symmetric magnetic interactions between CSRRs corresponding to cases (a) and (b), respectively.

corresponding to $k_z = \pi/a$, highlighted by the dotted black box.

The two cases discussed above represent the relative dipolar arrangements that occur at the highest and lowest frequencies of the passband where negative dispersion is exhibited by the 1D stack. With these configurations pinned at the band edges, all other possible combinations of dipolar arrangements occur at band frequencies between these edge frequencies. We next need to look at the negative dispersion in the CSRR stack because here we have both electric and magnetic field interactions to consider.

Based on the magnetic dipole orientation of the CSRR as depicted in Table I, the relative dipole orientations of the coupled magnetic dipoles will be transverse; the arrangement of these in the 1D stack are shown in Figs. 6(c) and 6(d), highlighted by the dotted red boxes. At $k_z = 0$, the magnetic dipoles form an antisymmetric pair. Referring back to Fig. 5, we see that they favor a lower-energy solution, thus competing with the electric field interaction that inclines towards a higher-energy solution in this case. Similarly, at $k_z = \pi/a$, the magnetic dipoles are symmetrically coupled favoring a higher-energy solution (see Fig. 5), once again competing with the electric field interaction that inclines towards a lower-energy solution. This competition between the electric and magnetic field interactions works to shift the edge frequencies towards the central frequency of the negative dispersion passband. The direct effect of this is a reduced interaction strength among the meta-atoms, a reduced resonant mode bandwidth [as seen in Fig. 2(b)], and a reduced group velocity (as seen in Fig. 3). Since the effect of magnetic interactions in the MNB-CSRR are suppressed owing to the lack of bianisotropy, the overall interelement interaction is stronger and hence the operational bandwidth is broader.

We briefly note that this coupled-dipole picture may at first appear slightly at odds with what one might expect. Typically, a negatively dispersing mode arises for *transversely* coupled dipoles since the in-phase arrangement of transverse coupled dipoles is the high-energy solution, while the out-of-phase arrangement, corresponding to a higher wave vector, is the lower-energy solution (seen from Fig. 5). This difference between initial expectations and the results we find here is a direct result of the need to consider the coupling between the *local* dipole moments on either side of the complementary ring systems rather than the *net* dipole moments as one would in other systems.

As a final point of discussion on the nature of the field interactions involved, we would like to step back from the dipole treatment and briefly consider the effect of near-field interactions. In an individual MNB-CSRR meta-atom, the zero net magnetic response is a consequence of the radiative cancellation of the magnetic fields between the atom's symmetric splits. However, when the separation between the MNB-CSRR meta-atoms in the stack is much smaller than the separation between the symmetric splits in each meta-atom, the near-field interactions between the adjacent meta-atoms dominate, resulting in a nonzero net magnetic field interaction strength. From Sec. III, it can be seen that the interelement separation of 1.5 mm chosen for the characterization of both metamaterial stacks, is about a factor of 11.5 (23) smaller than the transverse dimension of the CSRR (MNB-CSRR) meta-atoms. For the same interelement separation in the CSRR and MNB-CSRR stacks, the electric field interaction strength (mutual capacitance) is enhanced in the MNB-CSRR stack due to the greater transverse dimension of its meta-atoms. Despite the presence of some weak near-field magnetic effects, the enhanced electric field interaction in the MNB-CSRR stack assists in achieving a greater fractional bandwidth compared to the CSRR stack. This line of reasoning complements the ideas based on the coupled-dipole picture. In the competition between the electric and magnetic field interactions (even in the nonbianisotropic case), the dominant nature of the electric field interaction over the weak near-field magnetic interaction plays a key role in the enhanced fractional bandwidth of the MNB-CSRR stack.

In the next section, we compute the fractional bandwidth of the MNB-CSRR stack as a function of the longitudinal stacking period and compare it to that of the CSRR stack.

V. SENSITIVITY OF THE FRACTIONAL BANDWIDTH TO THE 1D PERIODICITY

As discussed in the previous section, the interelement interaction strength in the 1D CSRR stack is governed by both the electric and magnetic field interactions. While there are weak near-field magnetic interactions in the MNB-CSRR stack, the enhanced electric field interaction results in an increased fractional bandwidth. To analyze the sensitivity of the negative dispersive mode bandwidth in the CSRR and MNB-CSRR stacks, the dispersion relations of the two stacks were numerically computed in COMSOL MULTIPHYSICS, as

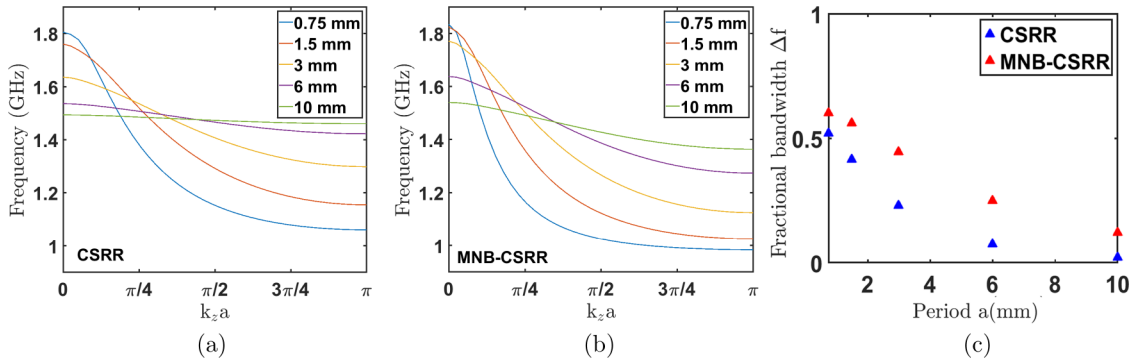

FIG. 7. Numerically computed dispersion relations for 1D stacks built from (a) CSRR meta-atoms and (b) MNB-CSRR meta-atoms plotting for changing 1D periodicity in the stacking direction, for period $a = 0.75$, 1.5, 3, 6, and 10 mm. At 10 mm, the frequency response of the CSRR stack is reduced to a highly narrow band. (c) The fractional bandwidth of the CSRR (blue curve) and MNB-CSRR (red curve) stacks plotted as a function of longitudinal periodicity, as calculated from Figs. 6(a) and 6(b). The fractional bandwidth of the MNB-CSRR stack is higher than the CSRR stack for all interelement separations.

a function of the period along the stacking direction. The spacing between the meta-atoms was completely filled with the substrate material to provide dielectric homogeneity.

Figures 7(a) and 7(b) present the numerically computed dispersion relations of the CSRR and the MNB-CSRR 1D stacks for period $a = 0.75$, 1.5, 3, 6, and 10 mm. It can be seen from Fig. 7(a) that at a period of 10 mm, the negative dispersive mode in the CSRR stack is reduced to a very narrow band. This behavior was already reported in [13] where the authors showed that upon increasing the period further, the dispersion can also become positive. From the analysis in [15] of interactions between coupled bianisotropic resonators, it could be understood that the flattening of the frequency band here might not be due to a lack of coupling between the meta-atoms. Rather, the balance between the electric and magnetic interaction strengths could cause the resonant states of the coupled meta-atoms in the system to be degenerate for a certain value of period causing the resonant band to flatten. As observed in [13], when the period is increased further, the higher- and lower-energy mode positions swap leading to a positive dispersion. It can be understood that this change in dispersing nature is caused by the shift in the balance between the two field interactions.

From figure 7(b), it is seen that the rate of decrease of the MNB-CSRR stack's fractional bandwidth is slower than that of the CSRR stack. At $a = 10$ mm, due to the decreased interaction strength among the meta-atoms, the fractional bandwidth of the MNB-CSRR has reduced to less than 0.2, as seen from figure 7(c), but still has not narrowed as much as that of the CSRR stack. The interaction strength in this system is dominated by the electric interaction, and the rate at which the mode bandwidth falls should directly relate to the decay length of the electric near-field of the meta-atoms. The transverse dimensions of the MNB-CSRR meta-atom are double that of the CSRR meta-atom so that the meta-atoms operate at the same resonance frequency. As already discussed, this change helps increase the stack's fractional bandwidth by enhancing the electric interaction strength (mutual capacitance) between MNB-CSRR meta-atoms.

The fractional bandwidth for the CSRR and MNB-CSRR stacks as computed from the dispersion relations in Figs. 7(a) and 7(b) is plotted in Fig. 7(c) as a function of the 1D stacking period. The immediate observation is that starting from a higher interelement separation (or period) and gradually decreasing it shows that at very small separations the fractional bandwidth of the MNB-CSRR stack does not continue increasing with the same trend as that of the CSRR, but instead saturates. This clearly demonstrates that at such small separations, the toy dipole interaction model does not include the effects of near-field interactions effectively. The general observation, however, is that irrespective of the chosen interelement separation, the fractional bandwidth offered by the MNB-CSRR stack is always higher than that of the CSRR stack.

From Sec. III, it was seen that the maximum transverse dimension (the truncated disk diameter) of the MNB-CSRR meta-atom is 34.4 mm, while that of the CSRR is 17.2 mm. Therefore, when the ratio of the maximum transverse dimension of a meta-atom to a given stacking period is calculated, it is found that this ratio for the 1D MNB-CSRR stack is double that for the 1D CSRR stack. From Fig. 7(c), it can be seen that when this ratio is the same for the CSRR and the MNB-CSRR stacks, for example, at $a = 3$ mm for the CSRR stack and at $a = 6$ mm for the MNB-CSRR stack, the fractional bandwidths of the two stacks are comparable, with that in the MNB-CSRR stack always somewhat higher. The similarity in bandwidth between the two stack types when account is taken of their different dimensions further supports the discussion above and suggests that the MNB-CSRR's greater transverse dimension for a given design frequency assists in enhancing the fractional bandwidth.

We experimentally demonstrated the MNB-CSRR metamaterial stack at a period $a = 1.5$ mm. This period was chosen specifically to increase the leakage of the field, thereby enabling the detection of the near fields and characterization of the dispersion relation. However, the plot in Fig. 7(c) shows that even at a reduced period $a = 0.75$ mm, a fractional bandwidth of 60.3% is achieved, which is an improvement over some of the existing configurations of magnetoinductive

waveguides, for example, the thin magnetoinductive cable proposed in [26].

VI. CONCLUSION

We have studied a negatively dispersing mode supported by a 1D metamaterial consisting of axially stacked MNB-CSRR meta-atoms and found that the experimentally determined mode dispersion is in good agreement with numerical simulations. We have also shown that the operational bandwidth of the mode is ultrawide and exceeds that offered by a similar system consisting of bianisotropic elements. Indeed, it exceeds that of any report we could find in the literature. We have employed a toy coupled-dipole model to show how the origin of negative dispersion in CSRR-based metamaterial devices can be understood, and used the same model to indicate how bianisotropy limits the maximum operational bandwidth. A study on the sensitivity of the operational bandwidth with stack period also revealed that the MNB-CSRR stack always offers a higher operational bandwidth in a given frequency range than the CSRR stack. Our results should be of assistance in the design of broadband metamaterial devices in such applications as wireless data transfer using metamaterials.

Data created during this research are openly available from the University of Exeters institutional repository [29].

ACKNOWLEDGMENTS

We acknowledge financial support from the Engineering and Physical Sciences Research Council (EPSRC) of the United Kingdom, via the EPSRC Centre for Doctoral Training in Metamaterials (Grant No. EP/L015331/1). W.L.B. acknowledges the support of the European Research Council through project Photmat (Grant No. ERC-2016-AdG-742222). I.R.H. acknowledges support from the EPSRC and QinetiQ Ltd. via the TEAM-A prosperity partnership (Grant No. EP/L015331/1). We also acknowledge GraphiC PLC for their assistance with the fabrication of samples for our experiments.

[1] V. G. Veselago, Sov. Phys.–Usp. **10**, 509 (1968).
[2] J. B. Pendry, A. J. Holden, D. J. Robbins, and W. J. Stewart, IEEE Trans. Microwave Theory Tech. **47**, 2075 (1999).
[3] D. R. Smith, W. J. Padilla, D. C. Vier, S. C. Nemat-Nasser, and S. Schultz, Phys. Rev. Lett. **84**, 4184 (2000).
[4] R. A. Shelby, D. R. Smith, and S. Schultz, Science **292**, 77 (2001).
[5] D. R. Smith, D. C. Vier, N. Kroll, and S. Schultz, Appl. Phys. Lett. **77**, 2246 (2000).
[6] R. R. A. Syms, E. Shamonina, V. Kalinin, and L. Solymar J. Appl. Phys. **97**, 064909 (2005).
[7] E. Shamonina, V. Kalinin, K. H. Ringhofer, and L. Solymar, Electron. Lett. **38**, 371 (2002).
[8] E. Shamonina, V. A. Kalinin, K. H. Ringhofer, and L. Solymar, J. Appl. Phys. **92**, 6252 (2002).
[9] M. J. Freire and R. Marqués, Appl. Phys. Lett. **86**, 182505 (2005).
[10] O. Sydoruk, M. Shamonin, A. Radkovskaya, O. Zhuromskyy, E. Shamonina, R. Trautner, C. J. Stevens, G. Faulkner, D. J. Edwards, and L. Solymar, J. Appl. Phys. **101**, 073903 (2007).
[11] F. Falcone, T. Lopetegi, M. A. G. Laso, J. D. Baena, J. Bonache, M. Beruete, R. Marqués, F. Martín, and M. Sorolla, Phys. Rev. Lett. **93**, 197401 (2004).
[12] M. Beruete, F. Falcone, M. J. Freire, R. Marqués, and J. D. Baena, Appl. Phys. Lett. **88**, 083503 (2006).
[13] M. Beruete, M. Aznabet, M. Navarro-Cía, O. E. Mrabet, F. Falcone, N. Aknin, M. Essaaidi, and M. Sorolla, Opt. Express **17**, 1274 (2009).
[14] M. A. Shapiro, S. Trendafilov, Y. Urzhumov, A. Alù, R. J. Temkin, and G. Shvets, Phys. Rev. B **86**, 085132 (2012).
[15] S. S. Seetharaman, C. G. King, I. R. Hooper, and W. L. Barnes, Phys. Rev. B **96**, 085426 (2017).
[16] J. D. Baena, J. Bonache, F. Martin, R. M. Sillero, F. Falcone, T. Lopetegi, M. A. G. Laso, J. Garcia-Garcia, I. Gil, M. F. Portillo, and M. Sorolla, IEEE Trans. Microwave Theory Tech. **53**, 1451 (2005).
[17] R. Marqués, F. Martín, and M. Sorolla, *Metamaterials with Negative Parameters: Theory, Design, and Microwave Applications* (Wiley, Hoboken, NJ, 2013).
[18] J. Naqui, Symmetry Properties in Transmission Lines Loaded with Electrically Small Resonators, Ph.D. thesis, Universitat Autònòma de Barcelona, 2014.
[19] R. Marqués, F. Medina, and R. Rafii-El-Idrissi, Phys. Rev. B **65**, 144440 (2002).
[20] J. D. Baena, L. Jelinek, R. Marqués, and J. Zehentner, Appl. Phys. Lett. **88**, 134108 (2006).
[21] J. D. Baena, L. Jelinek, and R. Marqués, Phys. Rev. B **76**, 245115 (2007).
[22] M. Noginov and V. Podolskiy, *Tutorials in Metamaterials* (CRC Press, Boca Raton, FL, 2011).
[23] C. É. Kriegler, M. S. Rill, S. Linden, and M. Wegener, IEEE J. Sel. Top. Quantum Electron. **16**, 367 (2010).
[24] C. Yeh and F. Shimabukuro, *The Essence of Dielectric Waveguides* (Springer, New York, 2006).
[25] F. Xu, K. Wu, and W. Hong, IEEE Trans. Microwave Theory Tech. **55**, 2502 (2007).
[26] R. R. A. Syms, L. Solymar, I. R. Young, and T. Floume, J. Phys. D: Appl. Phys. **43**, 055102 (2010).
[27] R. R. A. Syms, I. R. Young, and L. Solymar, J. Phys. D: Appl. Phys. **39**, 3945 (2006).
[28] N. Liu and H. Giessen, Angew. Chem., Int. Ed. **49**, 9838 (2010).
[29] S. S. Seetharaman, B. Tremain, W. Barnes *et al.*, Research data for "Realizing an ultra-wideband backward-wave metamaterial waveguide (dataset)," https://doi.org/10.24378/exe.944 (2018).